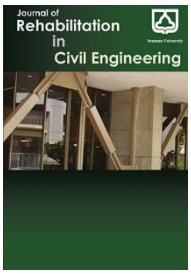

journal homepage: http://civiljournal.semnan.ac.ir/

Three-Mass Structural-Isolating-Damping Model Subjected to Near- and Far-Fault Earthquakes

Majid Amin Afshar[1], Mohammad Reza Adlparvar[2*], Sepehr Aghaei Pour[3]

1. Assistant Professor, Department of Technology and Engineering, Imam Khomeini International University, Qazvin, Iran
2. Associate Professor, Technical & Engineering Faculty, University of Qom, Qom, Iran
3. Ph.D. Student, Technical & Engineering Faculty, University of Qom, Qom, Iran
Corresponding author: *adlparvar@qom.ac.ir*

ARTICLE INFO

Article history:
Received: 26 January 2021
Revised: 01 March 2021
Accepted: 04 May 2021

Keywords:
Partially isolated (PI) structure;
Seismic isolator;
Damper;
Near-fault earthquake;
Far-fault earthquake.

ABSTRACT

Seismic base isolators and dampers are commonly used as control tools in building frames to mitigate earthquake damage. This study proposes and investigates a structural system consisting of a central fixed core and an isolated section, the two parts of which are connected to each other by a damper. In new structures, called partially isolated (PI) structures, the interaction between conventional frames with fixed bases and frames equipped with control tools including isolators and dampers is measured using a three-mass model by three simplified differential equations of motion. Validating the proposed model provided good results. The model with various modes of partial isolation and certain mass ratios was subjected to seven near-fault and seven far-fault earthquakes to be evaluated. The mean displacement, acceleration, and shear responses of the structural-isolating-damping model were compared with those of fully isolated (FI) and fully fixed (FF) structures. The results showed that by connecting the two parts, responses of the fixed part to FF structure and those of the isolated part to FI structure significantly improved. Under near-fault earthquakes, the displacement response reduction of the fixed part to FF model was estimated to be about 20% and the response of the isolated part to FI model was about 50%. Due to the functional weaknesses observed in FI structures including large displacement of the structure base, poor performance of the isolator in near-fault earthquakes, and high costs of preparing and installing the isolation system, these points were significantly resolved in PI structures.

How to cite this article:
Amin Afshar, M., Adlparvar, M., Aghaeipour, S. (2022). Three-Mass Structural-Isolating-Damping Model Subjected to Near- and Far-Fault Earthquakes. Journal of Rehabilitation in Civil Engineering, 10(1), 1-20.
https://doi.org/10.22075/jrce.2021.22466.1482

1. Introduction

Increasing population and industrial activities along with the lack of living spaces in cities have caused many high-rise buildings to be constructed adjacent to each other. These buildings are often constructed next to each other, either without any structural connection or by being connected only at the ground level. Therefore, the resistance of each structure to wind and earthquake loads is related solely to the same structure. Base isolation is a useful solution for reducing the seismic tendencies of a structure. Moreover, securing buildings via viscous dampers or energy dampers can be a good complement for the base isolation of buildings against earthquakes.

To mitigate the earthquake damage to adjacent structures, many studies have been conducted, in most of which the structures are connected by different types of dampers. Jangid and Bhaskararao studied adjacent Single-Degree-of-Freedom (SDOF) structures connected with friction dampers and found that dampers in elastic structures were more effective than stiff structures; as the damping of the elastic structure increased, the displacement of the dampers decreased significantly [1]. In another study, they connected SDOF structures by viscous dampers. The results showed that the damping of the connected structures had an alight effect on the optimum damping of the viscous dampers [2]. Jangid and Patel investigated the connected adjacent multi-degree-of-freedom (MDOF) structures and stated that dampers can be used only on some floors with the highest speed to minimize costs [3]. In analytical and laboratory studies, Basili et al. evaluated the performance of adjacent structures connected by MR dampers in both passive and semiactive modes. The results showed that optimum damping can be achieved without considering the number of stories. It was also observed that structural responses improved in the passive mode [4, 5]. Optimal arrangement of viscoelastic dampers and modal analysis of two structures connected by viscous dampers on the top floor have been carried out by Huang and Zhu [6] and Tubaldi [7], respectively. Tubaldi and co-authors in another research have investigated the performance of two adjacent structures connected by linear and nonlinear viscous dampers. They declared that by appropriate calibration of nonlinear viscous dampers, the responses decreased similar to the implementation of linear damper between structures [8].

Studying adjacent structures is not limited to the above cases. After selecting an appropriate damper, structure optimization is important. Optimizations have often been done based on multi-objective genetic algorithms and fuzzy logic [9, 10, and 11]. Most of the studies have focused on adjacent structures, the type of dampers, their junction, the height of structures, and instructions for selecting the optimal structural parameters and control tools.

Base isolation is used as a solution to reduce the vulnerability of buildings to earthquakes. In this case, two adjacent structures are connected by dampers. To the best of our knowledge, few studies have been conducted in this field. All the studies have dealt with the main problem of providing sufficient space for the motion of the isolated building. By connecting two adjacent structures using an active sensor in the highest part of the shorter structure and placing a seismic isolator under the base of one of the

structures, Fathi and Bahar observed that the best performance was achieved when the two structures remained within their elastic range and none of the frame elements showed a nonlinear behavior [12]. Shrimali et al. evaluated the isolation modes of a structure, i.e., with pneumatic rubber bearing and lead rubber bearing (LRB) isolators and without isolators. The results revealed that the structure equipped with LRB isolators had the least displacement, story shear, and impact between the two adjacent structures [13].

Matsagar and Jangid investigated the seismic response of adjacent MDOF structures in two modes of fixed-isolated and isolated-isolated. They argued that when both structures were isolated, large pier displacements, superstructure acceleration, and structural damage were greatly reduced [14]. In general, using control tools is among the well-known strategies to reduce the seismic hazards of multi-story buildings. Many ideas have also been proposed to reduce the response and evaluate the structure accurately, some of which are isolation in tall buildings [15], friction pendulum isolator in steel water tanks [16], partially reinforced raft foundation [17], combining a lead rubber bearing isolator and a TMD located in the base of the concrete structure [18], considering nonlinear inertia [19, 20], and floor isolation with springs and rollers from the main frame [21].

The common feature of all the previous studies has been in reducing the response of two adjacent structures by connecting them to each other using a damper, in some of which one structure is isolated from the ground, or using a special system to improve the response of a structure. However, the simultaneous use of isolators and dampers in new PI structures has received less attention [22]. By definition, this system has the same architecture as conventional structures, but from a structural point of view, it uses various lateral load-bearing systems. In this new approach, a part of the structural frame is isolated from the ground by seismic isolators and the other part is fixed to the ground; these two parts are connected by energy dissipation devices or dampers at the story level. Unlike previous research, the important point is the simultaneous use of isolators and dampers in the structure with the mentioned conditions.

Therefore, this study aims to present a three-mass structural-isolating-damping model to reduce the response of the structure. To do so, a main structure with known characteristics is considered. The part of the structure that is isolated from the ground is connected to the fixed part of the same structure with certain mass ratios. Accordingly, 15 models are obtained. For a more accurate evaluation, a fully isolated structure, as well as a fully fixed structure with similar characteristics to the main structure, is considered. All the models are subjected to seven near-fault and seven far-fault earthquakes and the minimum mean values of the maximum displacement, shear, and acceleration responses are provided. The mean responses of the three-mass structural-isolating-damping model in the form of a structure are compared with FF and FI structures.

2. Three-mass structural-isolating-damping model

In this section, a single-story structure is investigated, a part of which is isolated from the ground by a seismic isolator and upper deck, and the other part is fixed to the

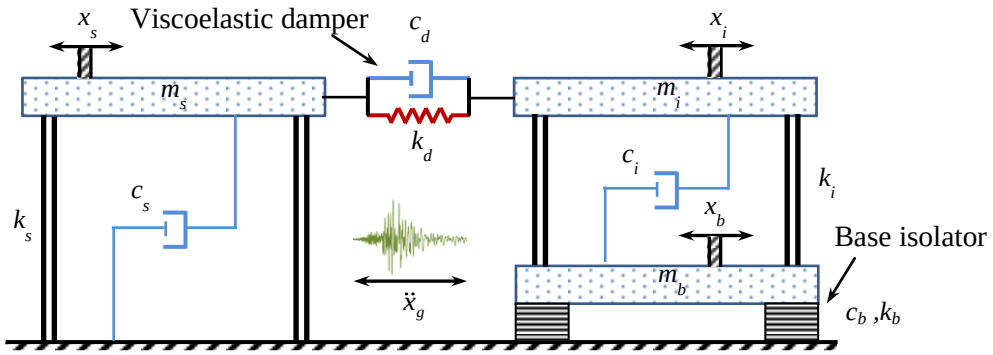

Fig. 1. Actual model of a single-story PI structure equipped with viscoelastic dampers.

ground. The two isolated and fixed cores are connected by viscoelastic dampers (Fig. 1). This structure is called a PI structure.

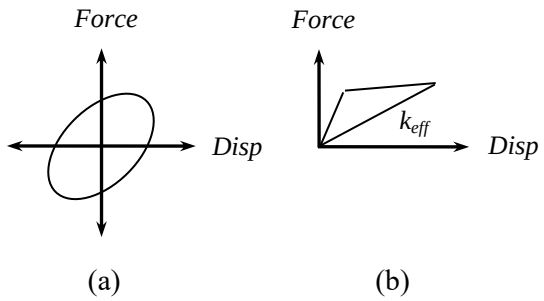

Fig. 2. Force-displacement curve in (a) damper and (b) isolator in three-mass model.

The behavior of bilinear seismic isolators along with equivalent stiffness and the performance of viscoelastic dampers were determined according to Kelvin-Voigt model presented in Fig. 2. The whole structure was considered to be symmetrical with symmetrical plates in its alignment and the roof of the structure was considered to be rigid. The mass-spring model, i.e., a three-mass model of the PI structure, is shown in Fig. 3.

The dynamic equation of motion of the structural-isolating-damping model was presented as follows:

$$\begin{bmatrix} m_b & 0 & 0 \\ 0 & m_i & 0 \\ 0 & 0 & m_s \end{bmatrix} \begin{Bmatrix} \ddot{x}_b \\ \ddot{x}_i \\ \ddot{x}_s \end{Bmatrix} + \begin{bmatrix} c_b + c_i & -c_i & 0 \\ -c_i & c_i + c_d & -c_d \\ 0 & -c_d & c_s + c_d \end{bmatrix} \begin{Bmatrix} \dot{x}_b \\ \dot{x}_i \\ \dot{x}_s \end{Bmatrix} + \begin{bmatrix} k_b + k_i & -k_i & 0 \\ -k_i & k_i + k_d & -k_d \\ 0 & -k_d & k_s + k_d \end{bmatrix} \begin{Bmatrix} x_b \\ x_i \\ x_s \end{Bmatrix} = -\begin{bmatrix} m_b & 0 & 0 \\ 0 & m_i & 0 \\ 0 & 0 & m_s \end{bmatrix} \begin{Bmatrix} 1 \\ 1 \\ 1 \end{Bmatrix} \ddot{x}_g \quad (1)$$

where m_b, m_i, and m_s denote the masses of the isolated deck, its superstructure, and the fixed part, respectively. k_s and c_s indicate the stiffness and damping of the fixed part, k_i and c_i represent the stiffness and damping of the isolated superstructure, k_b and c_b denote the stiffness and damping of the seismic isolator, and k_d and c_d show the stiffness and damping of the viscoelastic damping, respectively. The structure is placed in the fixed part, isolated superstructure, and isolated deck by x_s, x_i, and x_b displacements, respectively, with ground acceleration, $\ddot{x}_g$. Velocity and acceleration of each part of the structure are indicated by putting one ($\dot{}$) and two ($\ddot{}$)

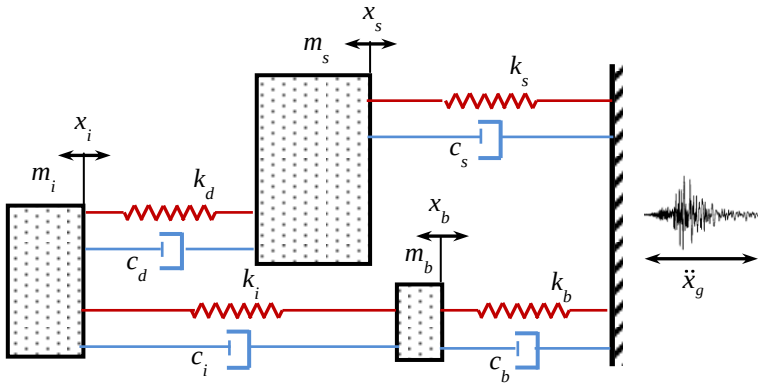

Fig. 3. Three-mass structural-isolating-damping model.

points over displacement quantities, respectively.

The frequency and damping ratio were calculated by Eqs. (2) and (3), respectively.

$$\omega_s = \sqrt{\frac{k_s}{m_s}} \qquad \omega_i = \sqrt{\frac{k_i}{m_i}}$$
$$\omega_b = \sqrt{\frac{k_b}{m_b}} \qquad \omega_d = \sqrt{\frac{k_d}{m_0}} \tag{2}$$

$$z_s = \frac{c_s}{2m_s\omega_s} \qquad z_i = \frac{c_i}{2m_i\omega_i}$$
$$z_b = \frac{c_b}{2m_b\omega_b} \qquad z_d = \frac{c_d}{2m_0\omega_0} \tag{3}$$

where ω_s and z_s denote the frequency and damping ratio of the fixed part, ω_i and z_i indicate the frequency and damping ratio of the isolated superstructure, ω_b and z_b represent the frequency and damping ratio of the seismic isolator, and ω_d and z_d denote the frequency and damping ratio of the viscoelastic damper, respectively.

In the above equations, due to the small mass of the viscoelastic damper, the structural characteristics of the viscoelastic damper (frequency and damping ratio) were measured relative to the main structure with mass m_0 and stiffness k_0. The mass of the main structure was equal to the sum of the mass of the isolated superstructure and the fixed part; this also applied to its stiffness. The frequency of the main structure, ω_0, was defined as $\omega_0 = \sqrt{k_0 / m_0}$.

3. Model validation

The new 3DOF structural-isolating-damping model was validated using Conner's SDOF model equipped with a tuned mass damper (TMD) under harmonic excitation $u_0e^{i\omega t}$ [23]. In Fig. 4 showing Conner's model, k and m denote the stiffness and mass of the undamped structure, respectively. m_d, c_d, and k_d show the mass, damping, and stiffness of the TMD system, respectively.

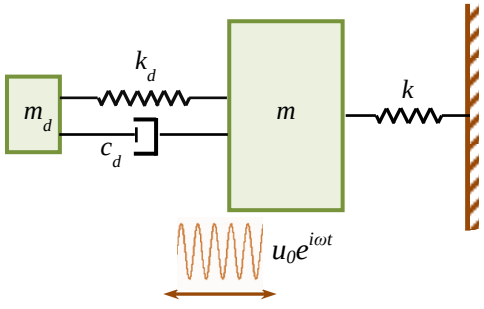

Fig. 4. Conner's SDOF model equipped with a TMD system.

The displacement response of the fixed part of the structure was obtained by placing the harmonic excitation in Eq. (1) and solving it by Eq. (4).

$$x_s = H_s \frac{u_0}{\omega_0^2} e^{i\omega t} \tag{4}$$

where u_0 and ω in harmonic excitation are the amplitude and frequency of the excitation, respectively. H_s is defined as the dynamic magnification factor of the fixed part of the structure and is the root of the fraction which its numerator and denominator are 4 degrees polynomial in accordance with z_d. Hence, the simplest form of H_s can be shown as follows:

$$H_s = \frac{\sqrt{a_1 z_d^4 + b_1 z_d^2 + c_1}}{\sqrt{a_2 z_d^4 + b_2 z_d^2 + c_2}} \tag{5}$$

The parameters a_1, b_1, c_1, a_2, b_2, and c_2 were obtained based on the simplified expressions presented in Table 1.

Table 1. Simplified expressions for determining viscoelastic damping coefficients.

Parameter	Definition
$\Omega_s = \omega_s / \omega_0$	Ratio of dimensionless frequency of the fixed part to the main structure
$\Omega_i = \omega_i / \omega_0$	Ratio of dimensionless frequency of the isolated part to the main structure
$\Omega_b = \omega_b / \omega_0$	Ratio of dimensionless frequency of the isolated deck to the main structure
$\Omega_d = \omega_d / \omega_0$	Ratio of dimensionless frequency of the damper to the main structure
$\mu_i = m_i / m_0$	Ratio of dimensionless mass of the isolated part to the main structure
$\mu_b = m_b / m_i$	Ratio of dimensionless mass of deck to the isolated superstructure
$\lambda = \omega / \omega_0$	Ratio of dimensionless frequency of harmonic excitation to the main structure
$q = z_b / z_d$	Damping coefficient (isolator-to-damper damping ratio)

Therefore, the coefficients of z_d in Eq. 5 (magnification factor of the fixed part) were calculated as follows:

$$a_1 = 16q^2\lambda^4\mu_b^2\Omega_b^2$$

$$b_1 = 8q\lambda^2\mu_b\left(-1+\mu_i\right)\mu_i\Omega_b\Omega_i^2\left(-\Omega_i^2+\mu_b\mu_i g_i^-\right)+ 4q^2\lambda^2\mu_b^2\Omega_b^2\left(\Omega_d^2+\mu_i g_i^-(\mu_i-1)\right)^2 + 4\lambda^2\left(\Omega_i^2+\mu_b\left(\mu_i\Omega_i^2-g_b^-\right)\right)^2$$

$$c_1 = \left(\begin{array}{l}\left(\lambda^2\mu_i(\mu_i-1)+\Omega_d^2\right)\Omega_i^2-\mu_b \\ \left(g_b^-\Omega_d^2+\mu_i^2 g_b^- g_i^- - \mu_i\left(\lambda^4-g_d^-\Omega_i^2-g_i^-\Omega_b^2\right)\right)\end{array}\right)^2$$

$$a_2 = 16q^2\lambda^4\mu_b^2\Omega_b^2\left(g_s^-+\mu_i\left(-\Omega_i^2+\Omega_s^2\right)\right)^2$$

$$b_2 = 8q\lambda^2\mu_b\left(-1+\mu_i\right)^2\mu_i\Omega_b\Omega_i^4\left(g_s^-\right)^2+4q^2\lambda^2\mu_b^2\Omega_b^2 \left(\Omega_d^2 g_s^- + \mu_i^2 g_i^- g_s^- + \mu_i\left(-\lambda^4+g_d^+\Omega_s^2+\Omega_i^2\left(g_d^- - \Omega_s^2\right)\right)\right)^2 + 4\lambda^2\left(\Omega_i^2\left(g_s^-+\mu_i\Omega_s^2\right)-\mu_b g_b^-\left(g_s^-+\mu_i\left(-\Omega_i^2+\Omega_s^2\right)\right)\right)^2$$

$$c_2 = \Omega_i^4\left(\Omega_d^2 g_s^- + \mu_i^2\lambda^2 g_s^- + \mu_i\left(-\lambda^4+g_d^+\Omega_s^2\right)\right)^2 - 2\mu_b g_b^-\Omega_i^2\left(\Omega_d^2 g_s^- + \mu_i^2\lambda^2 g_s^- + \mu_i\left(-\lambda^4+g_d^+\Omega_s^2\right)\right) \left(\Omega_d^2 g_s^- + \mu_i^2 g_i^- g_s^- + \mu_i\left(-\lambda^4+g_d^+\Omega_s^2+\Omega_i^2\left(g_d^- - \Omega_s^2\right)\right)\right) + \mu_b^2\left(g_b^-\right)^2 \left(\Omega_d^2 g_s^- + \mu_i^2 g_i^- g_s^- + \mu_i\left(-\lambda^4+g_d^+\Omega_s^2+\Omega_i^2\left(g_d^- - \Omega_s^2\right)\right)\right)^2$$

(6)

Where $g_k^{\pm} = \lambda^2 \pm \Omega_k^2$ and k subscript is considered s, i, b, and d.

In the Conner model, an undamped structure is connected to TMD with a specific mass, damping, and frequency. Given that the damper mass is often less than 5% of the mass of the main structure, the value of 1% was selected in the Conner model.

The mass ratio of the damper to the main structure is shown by $\bar{m}$ in the Conner model. In the study conducted by Conner, damping values of mass damper (z_{dc}) were considered to be 0, 0.03, and 1, and the damper-to-structure frequency ratio (f) was equal to 1. Index c in the mass damper represents the Conner model.

To simulate the three-mass model based on the Conner model, the isolated deck of the three-mass model was converted into a rigid body due to its absence in the Conner model and the frequency ratio of the isolated part was considered a small value, so as not to interfere with the frequency ratio of the viscoelastic damper. Hence, large values were selected for the three variables related to the isolated deck (Ω_b, μ_b, and q). Given that in the present study, the viscoelastic damper had a small mass, the mass of the isolated part along with the change of variable $\mu_i = \bar{m}/(1+\bar{m})$ was used to obtain the mass value of the mass damper in the Conner model. To calculate the frequency and damping of the viscoelastic damper, the change of variables $\Omega_d = f\sqrt{\mu_i}$ and $z_d = \mu_i f z_{dc}$ was used. The frequency ratio of the fixed part to the main structure (Ω_s) was considered to be 1.

Fig. 5 illustrates the changes in dynamic magnification factor of the fixed part of the three-mass model (H_s) relative to changes in the excitation frequency ratio (λ) at the damping values of 0.0001, 0.00031, and 0.0022. Fig. 4-15 in [23] indicated the changes in the dynamic magnification factor of the main structure relative to the changes in the frequency ratio of the mass damper at the damping values of 0, 0.03, and 1, which can also be seen in Fig. 5. The above damping values were selected for the viscoelastic damper in the three-mass model to better display the performance of the

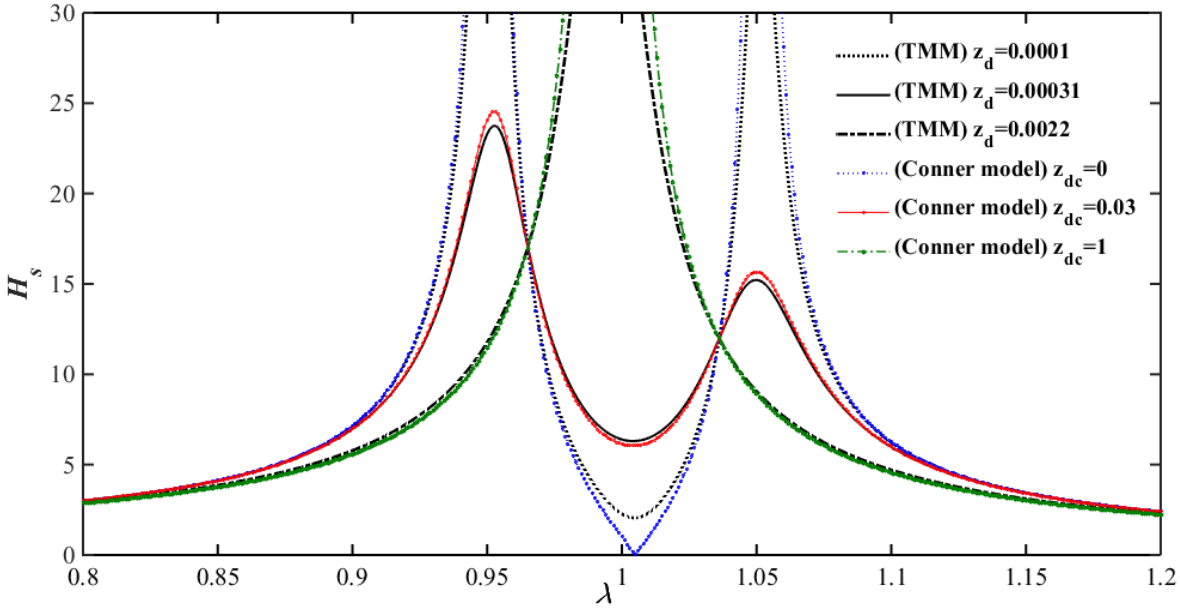

Fig. 5. Changes in dynamic magnification factor of the fixed part of the structure versus changes in excitation frequency ratio.

three-mass model compared to the Conner model. By placing the exact values of 0, 0.000297, and 0.0099, instead of damping values of the viscoelastic damper, the diagrams of the three-mass model completely matched the above-mentioned reference [23] diagrams. By simulating the new model based on the Conner model and changing the variables, the performance of the three-mass structural-isolating-damping model was optimal and validated.

4. Model evaluation

A structure with specific structural characteristics (stiffness and damping) was considered to evaluate the structural-isolating-damping system. Then, the isolated part was split from the part with fixed bases at different mass ratios. In connecting the structure with isolated bases and the structure with bases fixed to the ground, it is assumed that the lateral displacement of the isolation system was provided to prevent the collision of the two blocks. The three-mass models were subjected to 7 near-fault and 7 far-fault earthquakes; finally, the earthquake responses were averaged. The specifications of the studied models and earthquakes are described below.

4.1. Studied structures

For seismic design specification, AISC [24] (American institute of steel construction) and ASCE [25] (American Society of Civil Engineers) codes have been used. A two-dimensional single-story structure with 9 load-bearing pockets and 10 columns fixed to the ground was selected in California, U.S (Fig. 6). Both the span length and the contribution loading width perpendicular to each span were assumed to be 5 m. Dead and live loadings were 500 and 200 kg/m^2, respectively, with 20% live load contribution. The structure columns were 4 m high with the double cross-section of W8×15 and fixed bases. Due to the rigidity of the roof and its

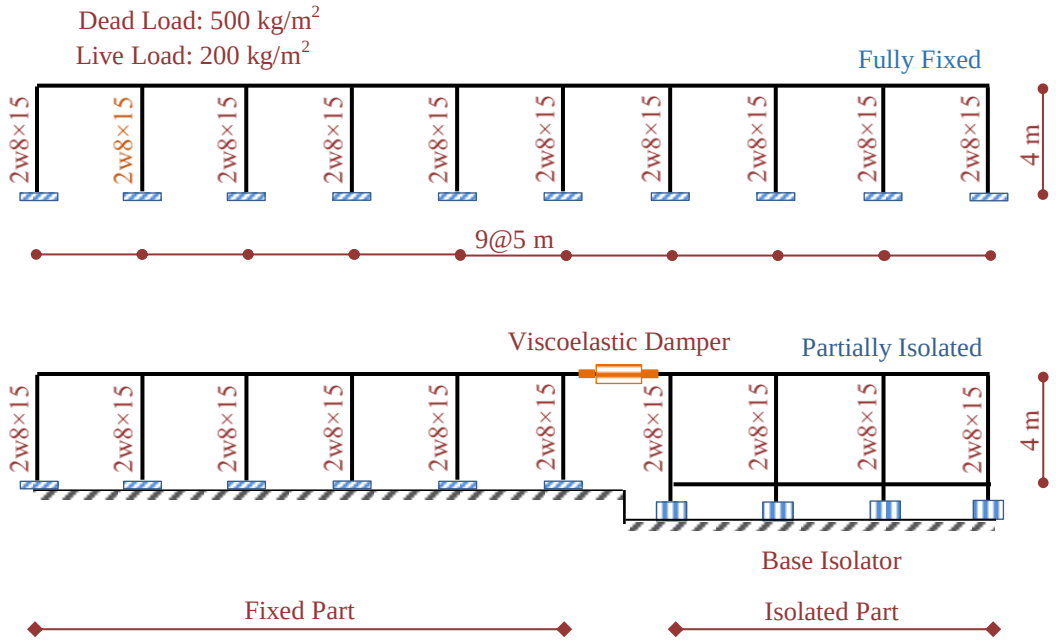

Fig. 6. Single-story structure with 10 columns under the condition of FF and PI.

shear structure, the total stiffness was obtained by combining the stiffness of the columns. Therefore, the total mass of the structure was obtained as 121.5 tons, the total stiffness of the structure was 1.5×10^6 kN/m, and the total damping ratio of the structure was 2%. In order to achieve a PI structure, the bases of a part of this structure were isolated from the ground by LRB isolators with a damping of 25%, and the two parts of the structure were connected by viscoelastic dampers. The mass ratio of the part isolated from the ground (m_i) to the main structure (m_0) is called the isolated mass ratio. The isolated mass ratios in the studied models were 0.01, 0.02, 0.05, 0.1 to 0.9 with increasing steps to 0.1, 0.95, 0.98, and 0.99. The two mass ratios of 0 and 1 indicated FF structures to the ground and FI structures, respectively. The isolated stiffness ratios were proportional to the isolated mass ratios. The selected isolators in FI structure were LRB with the damping of 25%. Damping of seismic isolators in three-mass models was determined according to coefficient μ_i and damping of the FI structure (25%).

The distribution of isolators per unit area was the same in all the models. The percentage distribution of isolators is defined as the ratio of the total surface area of all the isolators to the infrastructure surface of the isolated superstructure. Due to the same proportions of the isolator distribution in all the models, isolation frequencies and the mass ratio of the isolator deck were equal in all the structures. According to previous research [26], μ_b and Ω_b were considered to be 0.1 in all the models. Also, other structural and nonstructural characteristics of the models were considered to be similar.

4.2. Earthquake characteristics

To evaluate the structures, seven near-fault and seven far-fault accelerographs were taken from [27] and applied to the structures. Due to the structure placement in the high seismicity area (i.e. California), where intense earthquakes have occurred, the peak ground acceleration (PGA) values were scaled to 0.35 of gravitational acceleration (g) and, then, the structures were excited under scaled accelerographs [28]. Due to using seven earthquakes in each of the two near and far faults, the mean values of the responses were considered as the basis of evaluation. The applied excitations along with the year of occurrence, recording station, and peak acceleration and velocity of earthquakes for each of the near and far faults are presented in Tables 2 and 3, respectively.

Table 2. Characteristics of near-fault earthquakes.

Earthquake	Year	Recording station	PGA (g)	PGV (cm/s)
Bam	2003	Bam	0.81	124.2
Cape Mendocino	1992	Petrolia	0.66	88.5
Chi-Chi	1999	TCU102	0.3	91.7
Irpinia	1980	Sturno	0.32	72
Kobe	1995	KJMA	0.82	81.3
Loma Prieta	1989	Saratoga	0.51	41.6
Northridge	1994	Sylmar	0.84	129.6

Table 3. Characteristics of far-fault earthquakes.

Earthquake	Year	Recording station	PGA (g)	PGV (cm/s)
Bam	2003	Abaragh	0.17	4.7
Chi-Chi	1999	TCU045	0.51	46.4
Friuli	1976	Tolmezzo	0.36	22.9
Hachinohe	1968	Hachinohe-S252	0.23	40.7
Hector	1999	Hector Mine	0.33	44.8
Kobe	1995	Nishi-Akashi	0.48	46.8
Manjil	1990	Abbar	0.51	42.5

5. Performance of structures under near- and far-fault earthquakes

To analyze the performance of models, based on Eq. 1, Matlab software has been used. The equations have been solved numerically by implementing a numerical solver called ode45. The ode45 is the most perfect with high accuracy numerical solver of the various types of differential equations.

To achieve the responses of the isolated and fixed parts of the three-mass model under different dynamics characteristics (μ_i, Ω_d and, z_d), the following algorithm was created according to Fig 7. At first, a certain isolated mass ratio was specified. For this specified mass ratio, the frequency (Ω_{dj}) and damping (z_{dk}) values of the damper changed from 0 to 1 by step 0.01. Indices j and k denote the frequency and damping ratio counters, respectively. Then, each three-mass model was subjected to the excitations of near- and far-fault earthquakes. The time history diagrams of the displacement and acceleration responses of the isolated and fixed parts were plotted against time changes (denoted by $r(\mu_i, \Omega_{dj}, z_{dk}, \ddot{x}_g, t)$). Maximum response values were determined (denoted by $r_{j,k}^{\max}$).

At this point, for each three-mass model with specified μ_i, Ω_d and z_d, there were 7 maximum responses in near-fault earthquakes and also 7 maximum responses in far-fault earthquakes. Then, the maximum response values of each of near- and far-fault earthquakes were averaged separately (denoted by $\bar{r}$). For each specified μ_i, a 3D surface of the mean values of the maximums versus different Ω_d and z_d was attained, in which the minimum of this surface showed the coordinates of optimum frequency and damping (denoted by $\bar{r}_i^{opt}$ where i counts mass ratio). Due to repeating this procedure, the optimum responses for other μ_i besides the optimum values of FF and FI models were obtained.

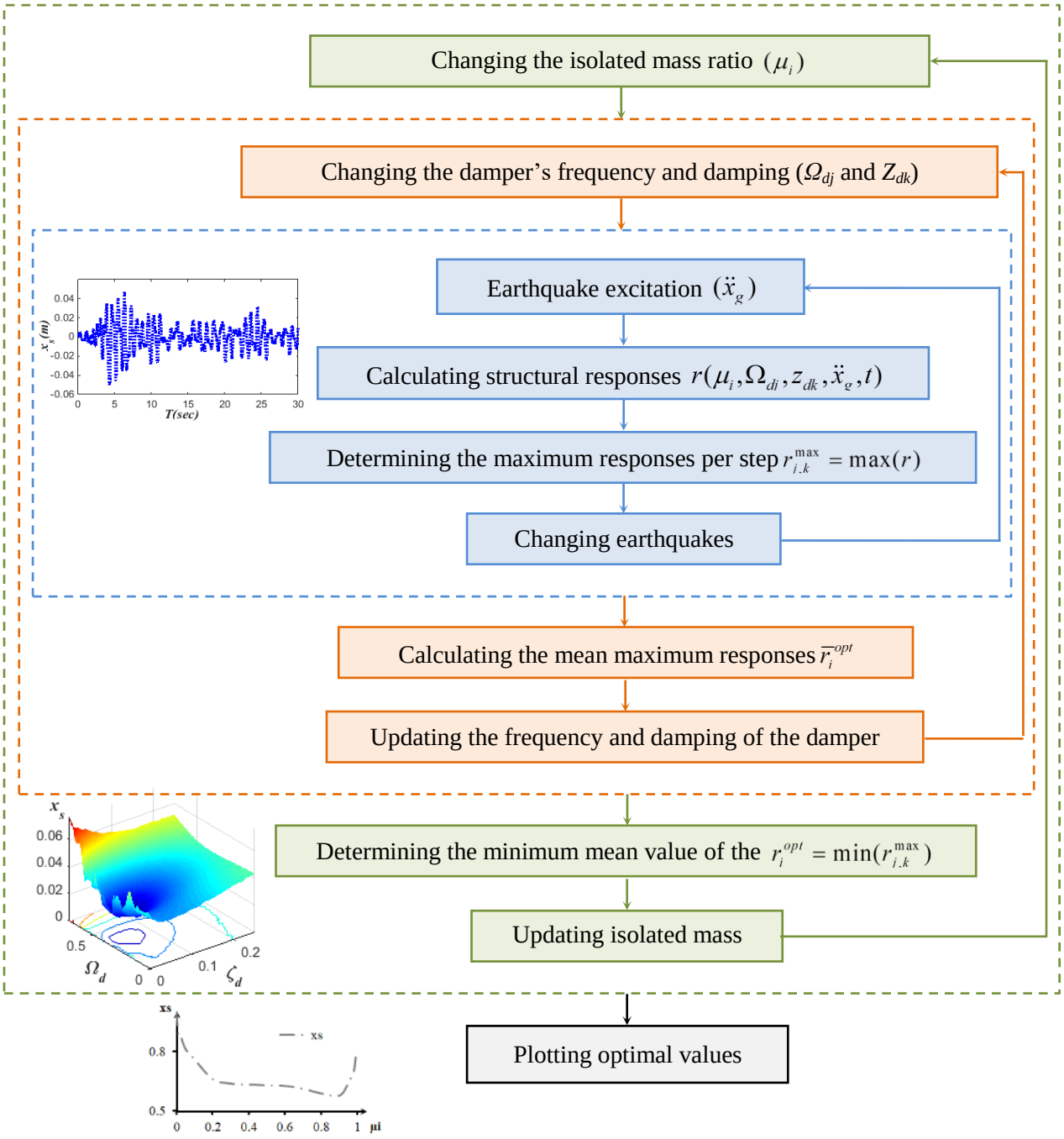

Fig. 7. Analysis process of PI structures.

To better understand the analysis process, the time history of displacement response under the Bam earthquake and the 3D procedure of the mean value of the maximum displacement responses are presented. Figs. 8 and 9 indicate displacement responses of the 50% isolated model under near- and far-fault accelerographs recorded for the Bam earthquake with damping and frequency ratios of 0.05 in the fixed and isolated parts, respectively. Displacement of the isolated part was the relative displacement of the superstructure from the lower deck. Displacement responses of both parts of the

structure in the near field showed larger values. As the time period of ground motions subjected to the Bam earthquake increased, the far-field responses manifested larger values than the near field. Displacement of the fixed part was significantly greater than the relative displacement of the isolated part.

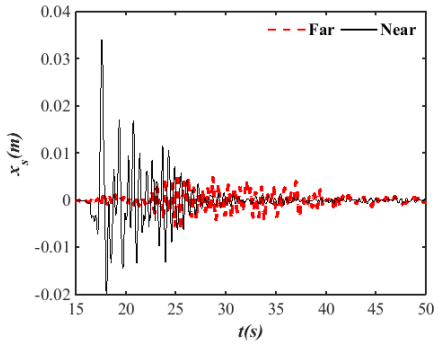

Fig 8. Time history of displacement of the fixed part under Bam near- and far-fault accelerograph

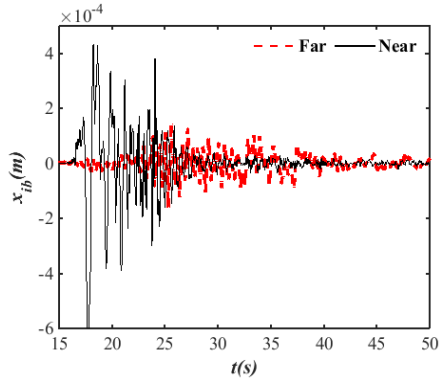

Fig. 9. Time history of relative displacement of the isolated part under Bam near- and far-fault accelerograph.

Figs. 10 and 11 illustrate the 3D procedure of the mean value of the maximum displacement of the fixed and isolated parts with changes in frequency and damping ratios under near- and far-field earthquakes, respectively. The closer the frequency and damping ratios to zero, the more optimal the displacement response of the fixed part in the near field and the isolated part in both fields would be. The minimum displacement response of the fixed part in the far-field was observed at the frequency ratio close to zero and the damping ratio of about 0.15. The maximum displacement response of both parts occurred at the frequency ratio of about 0.4 and the damping ratio close to zero in both fields. The mean value of the maximum responses of the fixed part showed much larger values than the isolated part.

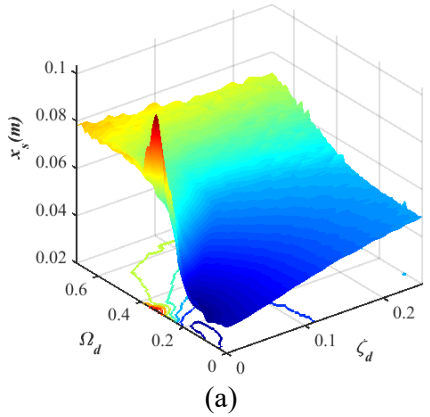

(a)

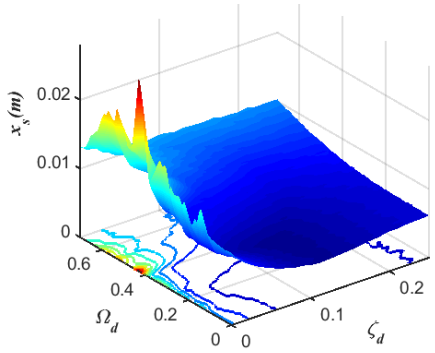

(b)

Fig. 10. Comparing the mean value of the maximum displacement responses of the fixed part along with the changes of frequency and damping ratios under (a) near- and (b) far-field earthquakes.

The FF and FI models were the same as the main structure with stiffness k_0 and mass m_0, which were fixed to the ground and isolated from the ground by seismic isolators, respectively. The dynamic equation of motion of the FF structure was obtained based on the equation of motion of the single-mass structure (SDOF) and the equation of motion of the FI structure was

obtained based on the equation of motion of the two-mass structure (including isolated deck and superstructure). Finally, the maximum responses including displacement, acceleration, and shear in the fixed and isolated parts were measured compared to the main fixed and isolated structure with changes at the isolated mass ratio.

According to the studied structures (15 structural-isolating-damping models and 2 FF and FI models), frequency and damping ratios of the damper (each 101 steps in PI models), and the near- and far-field earthquakes (14 earthquakes), the number of analyses was 2142238 to obtain accurate values of structural responses.

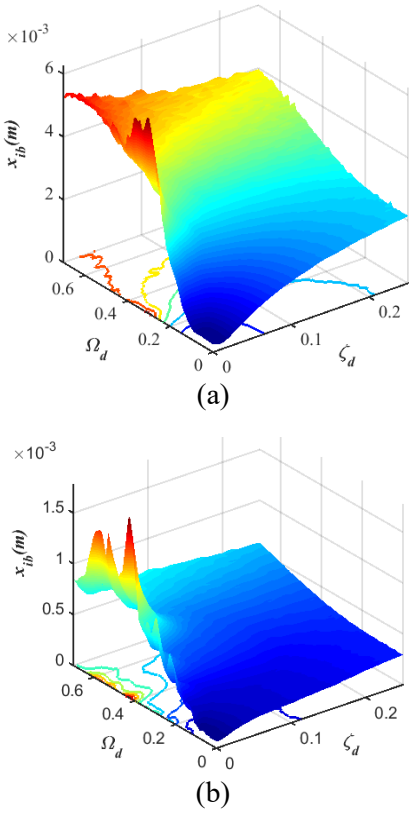

Fig. 11. Comparing the mean value of the maximum displacement responses of the isolated part along with the changes of frequency and damping ratios under (a) near- and (b) far-field earthquakes

5.1. Displacement responses

The displacement responses of the PI structure were investigated in three categories, including the fixed part to the ground, the isolated part from the ground, and the isolated deck. The displacement responses of the fixed part were dimensionless compared to the displacement responses of the FF model under near- and far-field earthquakes. Fig. 12 shows the optimal dimensionless displacement responses of the fixed part under near- and far-field earthquakes by the increase in isolated mass ratio. The responses under near- and far-field earthquakes are shown with solid and dashed lines, respectively. It was found that the relative mean values of displacement of the fixed part to FF structure were less than 1 at all the isolated mass ratios under near- and far-field earthquakes, such that displacement responses in near- and far-field earthquakes reduced by about 20% and 40%, respectively, suggesting the performance of the fixed part improved compared to the FF model. The minimum value of the maximum displacement responses under near-field earthquakes at μ_i between 0 and 0.2 decreased with a greater slope than at μ_i between 0.2 and 0.9. This slope was incrementally after μ_i exceeded 0.9. The mean dimensionless response under far-field earthquakes was lower than the near-field earthquakes. The mean displacement under far-fault earthquakes at μ_i between 0.2 and 0.8 was almost uniform and had a slope close to zero. The minimum value of the mean response under far-fault earthquakes occurred at μ_i equal to 0.5. In other words, if half of the structure is fixed to and the other half is isolated from the ground by seismic isolators, the displacement responses of the fixed part under far-fault earthquakes are optimal. The displacement

responses of the fixed part indicated that the performance of the fixed part was less favorable than the moderate rates of mass isolation if it was split to a very small or large extent.

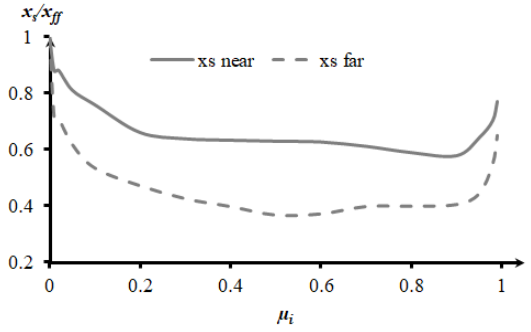

Fig. 12. The optimal mean value of the maximum dimensionless displacement responses of the fixed part under near- and far-fault earthquakes.

The minimum mean value of the maximum displacement responses of the isolated part was dimensionless compared to the FI model. The mean displacement response of the superstructure from the isolated deck in both PI and FI structures was reduced and was relative. Fig. 13 shows the optimal dimensionless displacement of the isolated part under near- and far-fault earthquakes. At moderate ratios of isolation, displacement responses of the isolated part reduced by about 50% in the near-fault and about 50% in the far fault compared to the FI model, suggesting that the isolated part had a more favorable behavior in near-fault earthquakes than far-fault earthquakes compared to the FI model. However, according to previous studies [29], the FI model alone under near-fault earthquakes demonstrated poorer performance and higher response values than the far-fault ones. Thus, it can be argued that by isolating only a part of the structure (compared to the full isolation), the poor behavior of the isolators can be improved under near-fault earthquakes.

As the isolated mass ratios increased, the displacement responses decreased, and this was more noticeable in near-field earthquakes than the far-field ones. At the largely isolated mass ratios, the displacement of the isolated part increased under both fields. The displacement responses of the isolated part showed that at moderate ratios of isolation, the model performance was optimal.

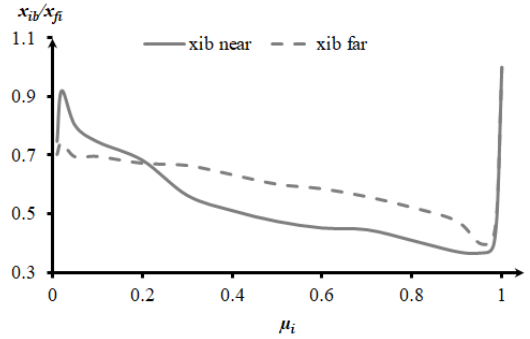

Fig. 13. The optimal mean value of the maximum dimensionless displacement responses of the isolated part under near- and far-field earthquakes.

The minimum mean value of the maximum deck displacement responses of the isolators in the PI structure was compared with the mean deck displacement response and design displacement of the isolation system in the FI structure (Fig. 14). The design displacement or maximum horizontal displacement of the isolation system was obtained by Eq. (7) [25].

$$D_D = \frac{gS_{D1}T_D}{4\pi^2 B_D} \tag{7}$$

where g is the acceleration of gravity, B_D is the coefficient which was equal to 1.6 according to the effective damping of the isolation system in the FI structure, and T_D is the effective time which was assumed to be 2 sec according to the stiffness and mass of the main structure. The spectral acceleration

parameter, S_{D1}, with the damping of 5% was obtained by Eq. (8):

$$S_{D1} = \frac{2}{3} F_V S_I \quad (8)$$

where F_v and S_I are site-related parameters with soil type D (because most of the accelerographs extracted soil type D), which were calculated as 1.5 and 0.6, respectively, based on the long-term T_D (1 sec) and site topographic maps (located in California).

In the PI structure, the mean displacement of the isolated deck under near-fault earthquakes was relatively higher than the far-fault ones. However, in the FI structure, the mean displacement under far-fault earthquakes was about 38% less than the near-fault ones. At moderate and low isolation ratios, it was found that the response of the PI model reduced more than that of the FI model in near-fault earthquakes compared to the far-fault ones. Although similar to the FI structure, the isolated part of the PI structure separated from the ground completely, it connects by the viscoelastic damper to the fixed part acting the same as a rigid wall. The more the isolated part tends to experience displacements, the more the damper damping is developed. Hence, the isolated part of the PI structure tends to have more displacements under near-fault earthquakes, but there is a larger opposing force from the damper that prevented the movement of the isolated part. Such manner wasn't observed stronger in the far-fault earthquakes because of lower vibration and lighter motion of the ground.

As the isolation ratio increased in the three-mass model, the displacement rate increased under both near- and far-fault earthquakes. The design displacement rate of the isolation system was equal to 18.6 and the deck displacement rate in the PI structure was less than 5 cm at ratios less than 50% of mass isolation. The lower the isolated mass ratio, the greater the difference in displacement between the PI structure and FI structure as well as the design displacement would be. This indicates that at moderate and low isolated mass ratios, large displacements, which are the main problem of the isolation system in FI structures, are significantly reduced and, consequently, more architectural space is provided in the plan of the isolated part. In other words, the plan area under operation increases as the space required to displace the isolators decreases.

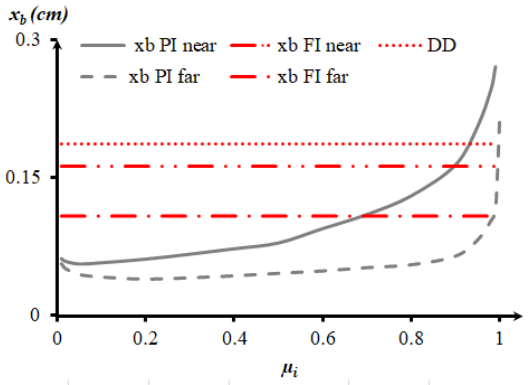

Fig. 14. The optimal mean value of the maximum responses of the deck displacement and design displacement of the isolation system under near- and far-fault earthquakes.

Fig. 15 shows the reduction rate of the isolated deck displacement response in the three-mass model relative to the design displacement under near- and far-fault earthquakes. The response reduction rate, *RP*, was obtained by Eq. 9:

$$RP = \frac{(D_D - x_{bpi})}{D_D} \times 100 \quad (9)$$

The response reduction rate under far-field earthquake was higher than the near-field earthquake and this rate decreased under both fields as the isolated mass ratio increased.

The response reduction rate was negative at μ_i more than 0.95 under near-field earthquake, indicating an increase in the isolated deck displacement relative to the design displacement. Isolating more than 0.95 of the PI structure did not show good performance under near-field earthquakes. The maximum response reduction rate under far-field earthquakes occurred at μ_i=0.2, while the maximum reduction rate under near-field earthquakes was observed at μ_i=0.1. The maximum RP rate under far-field earthquake was 8% greater than that under near-field earthquake.

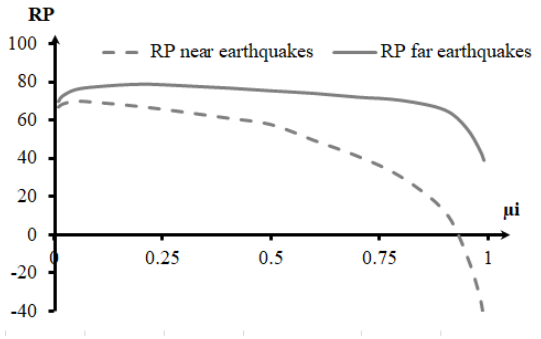

Fig. 15. The reduction rate of the optimal response of the isolated deck displacement under near- and far-field earthquakes.

5.2. Acceleration responses

The optimal mean value of the maximum acceleration of the fixed and isolated parts relative to that of FF and FI structures was dimensionless. Fig. 16 indicates the dimensionless acceleration in the fixed part under near- and far-field earthquakes. It can be observed that as the fixed area decreased or the isolated area increased, the acceleration of the fixed part decreased, such that with the proximity of the fixed part to the FF structure, the acceleration value approached zero. The mean acceleration values of the fixed part under near-field earthquake were higher than that of far-field and with increasing μ_i, the acceleration difference between the two fields decreased. The dimensionless acceleration of the fixed part indicated that the smaller the fixed area, the more optimal the responses would be.

Fig. 17 presents the mean value of the maximum dimensionless acceleration of the isolated part under near- and far-field earthquakes. The acceleration of the isolated part and FI structure was evaluated by the superstructure absolute acceleration. Changes in the acceleration of the isolated part under both near- and far-field earthquakes were almost uniform and constant, and dimensionless acceleration values under far-field earthquakes were slightly higher than those under the near-field ones, which suggested better performance of the isolated part under the near field than the FI structure. The mean dimensionless acceleration in the isolated part revealed that the acceleration changes were almost independent of the isolated and fixed areas, which was more evident under far-field earthquake.

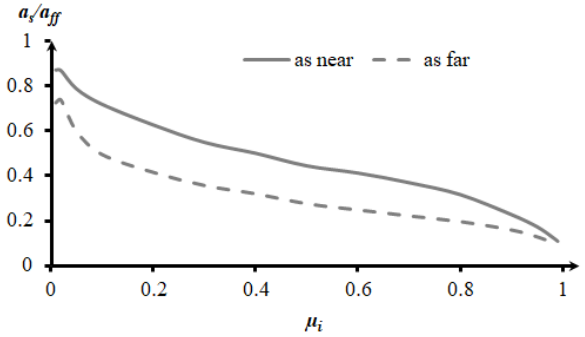

Fig. 16. The optimal mean value of the maximum dimensionless acceleration response of the fixed part under near- and far-field earthquakes.

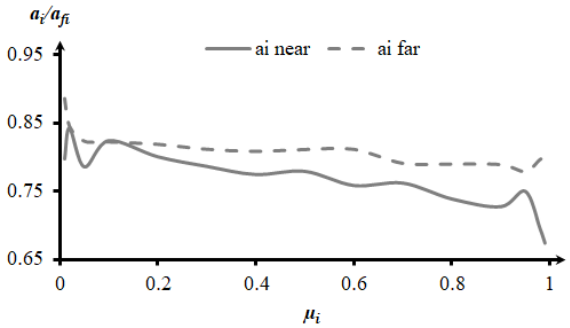

Fig. 17. The optimal mean value of the maximum dimensionless acceleration response of the isolated part under near- and far-field earthquakes.

5.3. Base shear responses

By analyzing the minimum mean value of the maximum shear response of structures, it was found that the fixed part compared to the FF model and the isolated part compared to the FI model were dimensionless. To achieve the base shear of each part in the models, the effect of the stiffness of that part on displacement was applied. The shear of FF and FI structures was obtained by multiplying the total stiffness by the displacement of the FF structure and the relative displacement of the isolated superstructure, respectively. Figs. 18 and 19 show the optimal dimensionless base shear in fixed and isolated parts under near- and far-field earthquakes, respectively.

Fig. 18 illustrates that, as the fixed area decreased, the relevant base shear rate decreased in the three-mass structural-isolating-damping model. This process continued to reach zero due to the stiffness reduction corresponding to the fixed part to increase the isolated mass rate. The difference in shear responses between near and far-fields started from 0.2 and, then, decreased to zero again with an increasing isolation ratio. Shear responses of the fixed part indicated that the performance of the fixed part was more desirable at high isolation ratios.

As can be seen in Fig. 19, as the isolated mass ratio increased, the shear responses of the isolated part increased due to the increased stiffness of the isolated part. This increase in responses under far-field earthquakes was more than that in the near-field ones, suggesting the better performance of the isolated part in the PI structure than the FI structure under near-fault earthquakes. In other words, by isolating a part of the structure and connecting it to the fixed part, the undesirable performance of the base shear of the isolated part under near-field earthquake can be prevented to some extent. In the most three-mass models, the shear responses of the isolated part in both near and far-fields are significantly less than those of the FI structure. At very high isolated mass ratios (close to one) or small fixed areas, the mean shear rate of the superstructure of the isolated part increases dramatically. However, these values reach zero at very small isolation ratios.

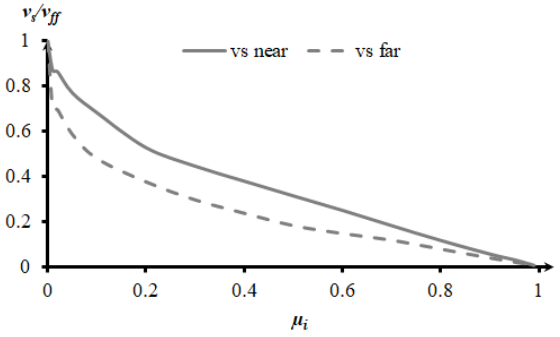

Fig. 18. The optimal mean value of the maximum dimensionless base shear response of the fixed part under near- and far-field earthquakes.

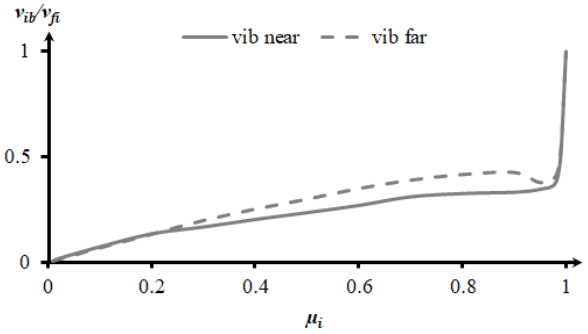

Fig. 19. The optimal mean value of the maximum dimensionless base shear response of the isolated part under near- and far-field earthquakes.

5. Conclusion

The three-mass model consisting of the isolated deck, the isolated superstructure, and the fixed structure was studied. The isolated part was connected to the fixed part by a viscoelastic damper. The similarity of the responses to the Conner's SDOF model equipped with TMD indicated that the model performance was optimal. To evaluate the model, a structure with specific structural characteristics was selected, the fixed part of which with various mass ratios was isolated from the other part of the structure (15 models). The models were subjected to the time history of seven near-fault and seven far-fault earthquakes with a wide range of damping and frequency ratios of the connecting damper. The minimum mean values of the maximum numerical responses of the fixed and isolated parts were dimensionless compared to the responses of the FF and FI structures, respectively. Responses included absolute displacement of the fixed part, the relative displacement of the isolated superstructure, absolute displacement of the isolated deck, absolute acceleration, and base shear of the fixed part and isolated superstructure.

The purpose of the optimization in this research is to find the minimum mean values of maximum responses of the FF, FI and, PI structural systems. Considering that the PI model complies with seismic code allowed restrictions, it also illustrates a behavior between the FF and FI structures resolving the economic and executive deficiencies of those structures. The evaluation results of the models are presented as follows:

1. Displacement of the fixed part reduced by 20% and 40% compared to the FF model under near- and far-fault earthquakes, respectively. Large displacement under the near-fault earthquake was among the weaknesses of seismic isolators. Displacement of the isolated part reduced more under near-fault than far-fault earthquakes compared to the FI model. The behavior of the isolated system when combined with the fixed part improved under near-fault earthquake.

2. Providing sufficient space for the displacement of isolators due to the occurrence of large displacements was another shortcoming of fully seismic isolators. At low to moderate isolated mass ratios, the isolated deck responses of the three-mass structural-isolating-damping model were above 50% less than that of the FI structure. The response decrease of the PI structure was observed under both the near- and far-field ground motions, compared to the design displacement values. In the new structural system, this weakness was resolved.

3. With increasing seismic isolated mass ratio, the acceleration responses of the fixed part decreased compared to the FF model. However, the process was uniform and unchanged in the isolated part compared to

the FI structure. The acceleration responses of the three-mass model were also reduced compared to FF and FI models.

4. The lower the isolation ratio, the higher and the lower the mean values of the maximum base shear responses in the fixed and isolated parts would be, respectively. The base shear responses in each part were directly correlated with the stiffness of that part. The base shear responses decreased in each part of the three-mass model compared to FI and FF structures.

In partial isolation of structures, the most balanced mode of isolation was to use the moderate isolation ratios. In other words, if about half of the structure is isolated from the ground by seismic isolators and the other half is fixed to the ground, more favorable results will be observed in responses of both parts. Due to the high cost of seismic isolation units, the new structure used a smaller number of isolators than FI structures, which was economical. Therefore, the three-mass structural-isolating-damping model, in addition to being economical compared to the FI model, also had a desirable performance.

Validation of this research was restricted to the demonstration of a numerical model and its validation under different earthquakes. It is obvious that this scheme requires experimental validation, as well.

REFERENCES

[1] Bhaskararao A., Jangid R. (2006). “Harmonic response of adjacent structures connected with a friction damper.” Journal of sound and vibration, Vol. 292, Issue 3, pp. 710-725.

[2] Bhaskararao A., Jangid R. (2007). “Optimum viscous damper for connecting adjacent SDOF structures for harmonic and stationary white-noise random excitations.” Earthquake engineering & structural dynamics. Vol. 36, Issue 4, pp. 563-571.

[3] Patel C., Jangid R. (2010). “Seismic response of adjacent structures connected with Maxwell dampers.” Asian journal of civil engineering. Vol. 11, Issue 5, pp. 585-603.

[4] Basili M., De Angelis M. (2007). “A reduced order model for optimal design of 2-mdof adjacent structures connected by hysteretic dampers.” Journal of Sound and Vibration. Vol. 306, Issue 1, pp. 297-317.

[5] Basili M., De Angelis M., Fraraccio G. (2013). “Shaking table experimentation on adjacent structures controlled by passive and semi-active MR dampers.” Journal of Sound and Vibration. Vol. 332, Issue 13, pp. 3113-3133.

[6] Huang X., Zhu H.-p. (2013). “Optimal arrangement of viscoelastic dampers for seismic control of adjacent shear-type structures.” Journal of Zhejiang University SCIENCE. Vol. 14, Issue 1, pp. 47-60.

[7] Tubaldi E. (2015). “Dynamic behavior of adjacent buildings connected by linear viscous/viscoelastic dampers.” Structural Control and Health Monitoring. Vol. 22, Issue 8, pp. 1086-1102.

[8] Tubaldi E., Gioiella L., Scozzese F., Ragni L., Dall'Asta A. (2020). “A design method for viscous dampers connecting adjacent structures.” Frontiers in Built Environment. Vol. 6, pp. 25.

[9] Uz M.E., Hadi M.N. (2014). “Optimal design of semi active control for adjacent buildings connected by MR damper based on integrated fuzzy logic and multi-objective genetic algorithm.” Engineering structures. Vol. 69, pp. 135-148.

[10] Kim H.-S. (2016). “Seismic response control of adjacent buildings coupled by semi-active shared TMD.” International Journal of Steel Structures. Vol. 16, Issue 2, pp. 647-656.

[11] Ok S.-Y., Song J., Park K.-S. (2008). “Optimal design of hysteretic dampers connecting adjacent structures using multi-objective genetic algorithm and stochastic

linearization method." Engineering structures. Vol. 30, Issue 5, pp. 1240-1249.

[12] Fathi F., Bahar O. (2017). "Hybrid Coupled Building Control for similar adjacent buildings." KSCE Journal of Civil Engineering. Vol. 21, Issue 1, pp. 265-273.

[13] Shrimali M., Bharti S., Dumne S. (2015). "Seismic response analysis of coupled building involving MR damper and elastomeric base isolation." Ain Shams Engineering Journal. Vol. 6, Issue 2, pp. 457-470.

[14] Matsagar V.A., Jangid R.S. (2005). "Viscoelastic damper connected to adjacent structures involving seismic isolation." Journal of civil engineering and management. Vol. 11, Issue 4, pp. 309-322.

[15] Reggio A., Angelis M.D. (2015). "Optimal energy-based seismic design of non-conventional Tuned Mass Damper (TMD) implemented via inter-story isolation." Earthquake Engineering & Structural Dynamics. Vol. 44, Issue 10, pp. 1623-1642.

[16] Abdeveis A., Mortezaei A.R. (2019). "Seismic Retrofitting the Steel Storage Tanks using Single Concave Friction Isolators under the Long Period Earthquakes." Journal of Rehabilitation in Civil Engineering. Vol. 7, Issue 2, pp. 40-53.

[17] Zhou F., Liu H., Mori M., Nobuo F., Zhu H. (2016). "Seismic response of a continuous foundation structure supported on partially improved foundation soil." Soil Dynamics and Earthquake Engineering. Vol. 90, pp. 128-137.

[18] De Domenico D., Ricciardi G. (2018). "Earthquake-resilient design of base isolated buildings with TMD at basement: application to a case study." Soil Dynamics and Earthquake Engineering. Vol. 113, pp. 503-521.

[19] Amin Afshar M., Aghaei Pour S. (2015). "Nonlinear Mechanic Model of Asymmetric Base-Isolated Structures Interaction against Harmonic Loads and Earthquake, and Study of Related Nonlinear Phenomena." Modares Mechanical Engineering. Vol. 14, Issue 16, pp. 152-162, (in Persian).

[20] Amin Afshar M., Aghaei Pour S. (2016). "On inertia nonlinearity in irregular-plan isolated structures under seismic excitations." Journal of Sound and Vibration. Vol. 363, pp. 495-516.

[21] Mahmoud H., Chulahwat A. (2015). "Response of building systems with suspended floor slabs under dynamic excitations." Engineering Structures. Vol. 104, pp. 155-173.

[22] Mazloum A.A., Amin Afshar M. (2020). "Study and comparison of seismic behaviour of isolator-damper hybrid control system with conventional structural systems." Journal of Rehabilitation in Civil Engineering. Vol. 8, Issue 2, pp. 01-17.

[23] Conner j.j., (2003). "Introduction to structural motion control." Pearson Education, Inc., United Kingdom.

[24] AISC Committee. (2010). "Specification for Structural Steel Buildings." American Institute of Steel Construction, Chicago-Illinois.

[25] A.S.o.C. Engineers, (2013). "Minimum Design Loads for Buildings and Other Structures." Standard ASCE/SEI 7-10, Amer Soc Of Civil Engin,.

[26] Naeim F. (2001). "Dynamics of Structures, Theory and Applications in Earthquake Engineering. Earthquake Spectra, Vol. 17, Issue 3, pp. 549-550.

[27] FEMA P695, (2009). "Quantification of building seismic performance factors." prepared by the applied technology council for the federal emergency management agency, Washington, D.C.

[28] Elnashai A. S., Di Sarno L. (2015). "Fundamentals of Earthquake Engineering." John Wiley & Sons, United States.

[29] Bhandari M., Bharti S., Shrimali M., Datta T. (2016). "PERFORMANCE OF BASE ISOLATED BUILDING FOR EXTREME EARTHQUAKES." structural engineering convention, Chennai, INDIA.